Auger and radiative deexcitation of P^{4+} ions

Kh Rezaul Karim, Mau Hsiung Chen, and Bernd Crasemann

Department of Physics and Chemical Physics Institute, University of Oregon, Eugene, Oregon 97403

X-ray wavelengths, Auger energies, and decay rates have been calculated for various states of the P^{4+} ion, with configurations $(1s^2 2s^2 2p^5)3s\,3p$, $3s\,3d$, $3p\,3d$, $3s^2$, $3p^2$, and $3d^2$. Intermediate coupling and configuration interaction have been taken into account. The energies and decay rates are found to be strongly affected by configuration interaction. The theoretical results are compared with recent observations in ion-atom collision experiments. Good agreement with measured spectra is found, and the calculations characterize a number of lines that had not previously been identified.

I. INTRODUCTION

The properties of highly stripped, excited atoms are very interesting from both theoretical and applied points of view. Intermediate coupling and configuration interaction must be incorporated in successful calculations, and measurements of transition energies and rates can constitute delicate tests of theory. Excited ions play important roles in certain laboratory plasma systems and in astrophysical processes, and metastable ionic states have been considered in connection with the design of short-wavelength lasers.

The difficulty in pursuing the theory of transitions in highly stripped atoms lies in the enormous number of possible initial states and the scarcity of experimental information against which calculations can be checked. Studies have consequently been limited to relatively few special cases.

One inviting system for theoretical analysis consists of highly ionized phosphorus and sulfur atoms with configurations of the form $1s^2 2s^2 2p^l 3s^m 3p^n$ ($l=3,4,5; m+n =2,3,4$), which have been studied in several recent ion-atom collision experiments.[1-4] In particular, Peterson *et al.* have resolved the multiplet structure in soft-x-ray spectra from Ne- and F-like S and P ions,[2] and Ridder and Schneider have made detailed measurements of the Auger-electron spectra produced in the excitation of P ions by thin carbon foils.[1] Only semiempirical estimates of term energies for some of these systems have been reported by Dahl *et al.*[4] Ridder and Schneider have performed Hartree-Fock calculations of the Auger electron energies,[1] but no calculations of x-ray energies and of transition rates have been reported so far, and configuration interaction has not previously been included. The present work is designed to fill this gap in the body of available calculations.

Among the large number of conceivable initial configurations, we restrict ourselves to P^{4+} with $1s^2 2s^2 2p^5 3s^m 3p^n 3d^q$, $m+n+q=2$. This leaves us with six initial configurations, viz., $(1s^2 2s^2 2p^5)3s\,3p$, $3s\,3d$, $3p\,3d$, $3s^2$, $3p^2$, and $3d^2$. Angular momentum coupling among the electrons in the unfilled shells leads to a multitude of possible initial states $|\,l^n(S_n L_n)l'^m(S_m L_m)S_{12}L_{12}l''^t(S_t L_t)SLJM\rangle$. These

states decay predominantly through Auger and $E1$ radiative transitions. We report on Hartree-Slater calculations of x-ray and Auger transition rates and energies for all such states, computed in intermediate coupling[5] with configuration interaction.[5,6] The results permit identification of lines in the observed spectra. The computations follow the lines of previous related studies by our group.[7-10]

II. THEORY

The x-ray and Auger transition rates were calculated from time-dependent perturbation theory:

$$W=(2\pi/\hbar)\,|\,\langle\psi_f\,|\,A\,|\,\psi_i\rangle\,|^2\rho(E_f)\,,\qquad(1)$$

where ψ_i and ψ_f are the initial and final states of the system, respectively, and $\rho(E_f)$ is the density of final states. Because many electrons and several open shells are involved, the calculation of the matrix elements $\langle\psi_f\,|\,A\,|\,\psi_i\rangle$ is not trivial. Calculational techniques for such systems were initiated by Racah[11] and developed by others.[12,13] In our calculation we followed the technique suggested by Fano.[12]

A. X-ray emission rates

The transition probability for spontaneous emission of a photon of angular frequency ω is[14]

$$W=\frac{4\omega^3}{3\hbar c^3}\frac{1}{2J+1}\,|\,\langle\gamma'J'||D||\gamma J\rangle\,|^2\,,\qquad(2)$$

where γJ and $\gamma'J'$ represent the initial and final states of the system, respectively, D is the electric-dipole operator, and $\langle\gamma'J'||D||\gamma J\rangle$ is the reduced matrix element.

Ignoring the two closed shells for the time being, the configurations of the P^{4+} ion can be written as $l^n l'^m l''^t$, where l represents the $2p$ subshell, and l' and l'' may represent any of the remaining $3s$, $3p$, or $3d$ subshells. This system can decay through electric-dipole transitions to (i) $l^{n+1}l'^{m-1}l''^t$ or (ii) $l^{n+1}l'^m l''^{t-1}$ producing L x rays, and to (iii) $l^n l'^{m+1}l''^{t-1}$ producing M x rays. The reduced matrix element of type (i) is

$$\langle \gamma'J'||D||\gamma J\rangle = (-1)^{m-1}[m(n+1)]^{1/2}(-1)^\delta$$

$$\times [J,J',L,L',L_{12},L'_{12},S_m,L_m,S'_n,L'_n]^{1/2}\delta_{SS'}\delta_{S_t}\delta_{S'_t}\delta_{S_{12}S'_{12}}\delta_{L_tL'_t}$$

$$\times \langle l'^m S_m L_m\{|l'^{m-1}S'_m L'_m\rangle\langle l^{n+1}S'_n L'_n\{|l^n S_n L_n\rangle$$

$$\times \begin{Bmatrix} J' & 1 & J \\ L & S & L' \end{Bmatrix} \begin{Bmatrix} S_{12} & S_n & S_m \\ \tfrac{1}{2} & S'_m & S'_n \end{Bmatrix} \begin{Bmatrix} L'_{12} & L' & L_t \\ L & L_{12} & 1 \end{Bmatrix} \begin{Bmatrix} L_n & L_{12} & L_M \\ l & 1 & l' \\ L'_n & L'_{12} & L'_m \end{Bmatrix} \langle l||D||l'\rangle \,, \tag{3}$$

where we have

$$|\gamma J\rangle \equiv |l^n(S_n L_n)l'^m(S_m L_m)S_{12}L_{12}l''^t(S_t L_t)SLJ\rangle \,, \tag{4}$$

$$|\gamma'J'\rangle \equiv |l^{n+1}(S'_n L'_n)l'^{m-1}(S'_m L'_m)S'_{12}L'_{12}l''^t(S'_t L'_t)S'L'J'\rangle \,, \tag{5}$$

$$\delta = S+J'+L_t+S_n+2S'_m-S_m+S_{12}+L_n+L_{12}+l+L'_n \,, \tag{6}$$

and

$$\langle nl||D||n'l'\rangle = -e\int R_{nl}R_{n'l'}rr^2dr(-1)^{l+(l+1+l')/2}l_{\max}^{1/2} \,, \quad l'=l\pm1 \,. \tag{7}$$

Transitions of type (ii) were encountered only in the somewhat simpler form $[l^{-1}]l'l''\rightarrow l^{n_0}l'$, for which the reduced matrix element is

$$\langle \gamma'J'||D||\gamma J\rangle \equiv \langle l^{n_0}l'S'L'J'||D||[l^{-1}]^2ll'S_{12}L_{12}l''SLJ\rangle$$

$$=2^{-1/2}(-1)^{S+L+J'+L_{12}+l'+l''}[S_{12},L_{12},J,J',L]^{1/2}\begin{Bmatrix} l' & L & 1 \\ J & J' & \tfrac{1}{2} \end{Bmatrix}\begin{Bmatrix} l & l'' & 1 \\ L & l' & L_{12} \end{Bmatrix}\langle l||D||l''\rangle\delta_{S1/2} \,, \tag{8}$$

where the symbols l^{n_0} and $[l^{-1}]$ indicate a closed shell and a shell closed but for one electron, respectively.

The transitions of type (iii) were found to proceed via two simpler schemes: $l^n l''^t\rightarrow l^n l'l''^{t-1}$ and $l^n l'l''\rightarrow l^n l'^2$; the reduced matrix elements for these cases are

$$\langle \gamma'J'||D||\gamma J\rangle \equiv \langle l^n(S'_n L'_n)l'[^2l']S_{12}L'_{12}l''^{t-1}(S'_t L'_t)S'L'J'||D||l^n(S_n L_n)l''^t(S_t L_t)SLJ\rangle$$

$$=(-1)^{t-1}t^{1/2}(-1)^\delta\langle l''^t S_t L_t\{|l''^{t-1}S'_t L'_t,l''_N\rangle[J,J',L,L',S_t,L_t,S'_{12},L'_{12}]^{1/2}\delta_{SS'}$$

$$\times \begin{Bmatrix} J' & 1 & J \\ L & S' & L' \end{Bmatrix}\begin{Bmatrix} S'_t & S & S'_{12} \\ S_n & \tfrac{1}{2} & S_t \end{Bmatrix}\begin{Bmatrix} L'_t & l''_N & L_t \\ L' & 1 & L \\ L'_{12} & l' & L_n \end{Bmatrix}\langle l'||D||l''\rangle \,, \tag{9}$$

where

$$\delta = S_n+2S'_t+2S+1-S_t+J'+L'+L'_{12}+l'+L_n \,, \tag{10}$$

and

$$\langle \gamma'J'||D||\gamma J\rangle \equiv \langle l^n(S_n L_n)l'^2(S'_m L'_m)S'L'J'||D||l^n(S_n L_n)^2l'S_{12}L_{12}^2l''SLJ\rangle$$

$$=\sqrt{2}(-1)^\delta\langle l'^2 S'_m L'_m\{|l'(^2l')l'_N\rangle[J,J',L,L',S'_m,L'_m,S_{12},L_{12}]^{1/2}\delta_{SS'}$$

$$\times \begin{Bmatrix} S_n & \tfrac{1}{2} & S_{12} \\ \tfrac{1}{2} & S' & S'_m \end{Bmatrix}\begin{Bmatrix} L_n & l' & L_{12} \\ l'_N & L' & L'_m \end{Bmatrix}\begin{Bmatrix} J' & 1 & J \\ L & S' & L' \end{Bmatrix}\begin{Bmatrix} L' & 1 & L \\ l'' & L_{12} & l'_N \end{Bmatrix}\langle l'||D||l''\rangle \,, \tag{11}$$

where

$$\delta = 2S'+L+J'+L_{12}+l''+S_n+L_N+1 \,. \tag{12}$$

B. Auger transition rates

Matrix elements for the two-electron interaction operator $V=\sum_{i>j}1/r_{ij}$ can be expressed as a weighted sum of radial Slater integrals,

$$\langle \psi \mid V \mid \psi' \rangle = \sum_k a_k R^k(n_1l_1,n_2l_2;n_3'l_3',n_4'l_4') .$$

Fano[12] used Racah algebra to determine the angular coefficients a_k for a many-electron atom with several open shells. Fano's formulation has been incorporated into a computer program by Hibbert.[15] We have computed the angular coefficients using Hibbert's angular momentum integral code.[15] Herman-Skillman[16]—Hartree-Slater wave functions were used to calculate the Slater integrals.

C. Spin-orbit interaction

The spin-orbit interaction matrix element for the configuration $l^n l'{}^m l''{}^t$ was derived following Wybourne[17]

$$\langle l^n(S_nL_n)l'{}^m(S_mL_m)S_{12}L_{12}l''{}^t(S_tL_t);SLJM \mid H_{SO} \mid l^n(S_n'L_n')l'{}^m(S_m'L_m')S_{12}'L_{12}'l''{}^t(S_t'L_t'); S'L'JM \rangle$$

$$=(-1)^{J+L+S'}\begin{Bmatrix} L & L' & 1 \\ S' & S & J \end{Bmatrix}(A_{nl}\xi_{nl}+A_{n'l'}\xi_{n'l'}+A_{n''l''}\xi_{n''l''}) , \qquad (13)$$

where

$$A_{nl}=(-1)^{\delta_1}[L,L',S,S',L_{12},L_{12}',S_{12},S_{12}']^{1/2}[l(l+1)(2l+1)]^{1/2}$$

$$\times \begin{Bmatrix} L_{12} & L & L_t \\ L' & L_{12}' & 1 \end{Bmatrix}\begin{Bmatrix} S_{12} & S & S_t \\ S' & S_{12}' & 1 \end{Bmatrix}\begin{Bmatrix} L_n & L_{12} & L_M \\ L_{12}' & L_n' & 1 \end{Bmatrix}\begin{Bmatrix} S_n & S_{12} & S_m \\ S_{12}' & S_n' & 1 \end{Bmatrix}$$

$$\times \delta_{L_tL_t'}\delta_{S_tS_t'}\delta_{L_mL_m'}\delta_{S_mS_m'}\langle l^n\alpha S_nL_n||V^{(11)}||l^n\alpha'S_n'L_n' \rangle , \qquad (14)$$

$$A_{n'l'}=(-1)^{\delta_2}[S,S',L,L',L_{12},L_{12}',S_{12},S_{12}']^{1/2}$$

$$\times \begin{Bmatrix} S_{12} & S & S_t \\ S' & S_{12}' & 1 \end{Bmatrix}\begin{Bmatrix} L_{12} & L & L_t \\ L' & L_{12}' & 1 \end{Bmatrix}\begin{Bmatrix} L_m & L_m' & 1 \\ L_{12}' & L_{12} & L_n \end{Bmatrix}\begin{Bmatrix} S_m & S_m' & 1 \\ S_{12}' & S_{12} & S_n \end{Bmatrix}\delta_{S_tS_t'}\delta_{L_tL_t'}\delta_{S_nS_n'}\delta_{L_nL_n'}$$

$$\times [l'(l'+1)(2l'+1)]^{1/2}\langle l'{}^m\alpha S_mL_m||V^{(11)}||l'{}^m\alpha'S_m'L_m' \rangle , \qquad (15)$$

$$A_{n''l''}=(-1)^{\delta_3}[S,S',L,L']^{1/2}[l''(l''+1)(2l''+1)]^{1/2}$$

$$\times \begin{Bmatrix} S_t & S_t' & 1 \\ S' & S & S_{12} \end{Bmatrix}\begin{Bmatrix} L_t & L_t' & 1 \\ L' & L & L_{12} \end{Bmatrix}\delta_{S_{12}S_{12}'}\delta_{L_nL_n'}\delta_{L_mL_m'}\delta_{S_nS_n'}\delta_{L_{12}L_{12}'}\delta_{S_mS_m'}\langle l''{}^t\alpha S_tL_t||V^{(11)}||l''{}^t\alpha'S_t'L_t' \rangle , \qquad (16)$$

$$\delta_1=L_{12}+L_t+L'+S_{12}+S'+L_n+L_m+L_{12}'+S_n+S_m+S_{12}'+S_t , \qquad (17)$$

$$\delta_2=2S_{12}+S_t+S'+L_t+L'+L_n'+L_m'+S_n'+S_m' , \qquad (18)$$

$$\delta_3=S_{12}'+S_t'+S+L_{12}'+L_t'+L , \qquad (19)$$

and

$$\langle l^n\alpha S_nL_n||V^{(11)}||l^n\alpha'S_n'L_n' \rangle = n(\tfrac{3}{2})^{1/2}[S_n,L_n,S_n',L_n']^{1/2}\sum_{\bar{S},\bar{L}}\{(l^nS_nL_n[\mid l^{n-1}\bar{S}\bar{L})(l^{n-L}\bar{S}\bar{L}\mid]l^nS_n'L_n'\}$$

$$\times \begin{Bmatrix} S_n & S_n' & 1 \\ \frac{1}{2} & \frac{1}{2} & \bar{S} \end{Bmatrix}\begin{Bmatrix} L_n & L_n' & 1 \\ l & l & \bar{L} \end{Bmatrix}(-1)^{\bar{S}+\bar{L}+S_n+L_n+l+1/2} . \qquad (20)$$

III. NUMERICAL CALCULATIONS

The Herman-Skillman—Hartree-Slater model[16] was used to generate the single-particle wave functions from which the radial integrals were calculated. The six configurations listed in Sec. I give rise to 174 possible initial states ϕ_i. These ϕ_i served as the basis set for constructing a matrix representation for the total Hamiltonian

$$H=\sum_i \left[-\frac{\hbar^2}{2m}\nabla_i^2 -\frac{Ze^2}{r_i} +\sum_{i>j}\frac{e^2}{r_{ij}} -\xi(r_i)\bar{l}_i\cdot\bar{s}_i \right] . \qquad (21)$$

We used the expressions derived in Sec. II to calculate the individual matrix elements $\langle \phi_j \mid H \mid \phi_i \rangle$ of this Hamiltonian. The wave functions $\psi_i = \sum_j c_{ij}\phi_j$ were then obtained by diagonalizing the matrix. These wave functions were then used to calculate the transition probabilities.

TABLE I. Auger and x-ray transition rates (in atomic units), Auger energies (in eV), and x-ray wavelengths (in Å) of states of the P^{4+} ion. Numbers in parentheses indicate powers of 10, e.g., $0.0443(-5)=0.443\times10^{-5}$.

Principal component	Auger transitions to $2p^6\epsilon s$		L-x-ray transition to $2p^63p$		Total M-x-ray rate
	Energy	Rate	Wavelength	Rate	
$2p^53p\,(^3D)3d\,^2P$	109.75	0.634(-4)	75.98	0.544(-6)	0.447(-7)
$2p^53p\,(^3D)3d\,^2S$	108.68	0.373(-3)	76.48	0.181(-5)	0.353(-7)
$2p^53p\,(^1D)3d\,^2P$	107.13	0.489(-6)	77.23	0.206(-5)	0.703(-7)
$2p^53p\,(^1D)3d\,^2S$	106.21	0.223(-3)	77.67	0.655(-6)	0.359(-7)
$2p^53p\,(^1P)3d\,^2P$	105.64	0.551(-6)	77.95	0.997(-7)	0.511(-7)
$2p^53p\,(^3P)3d\,^4P$	105.48	0.137(-3)	78.03	0.410(-6)	0.360(-7)
$2p^53p\,(^3D)3d\,^4D$	104.89	0.259(-5)	78.32	0.127(-6)	0.376(-7)
$2p^53p\,(^3P)3d\,^4D$	104.06	0.924(-7)	78.73	0.123(-7)	0.508(-7)
$2p^53p\,(^3D)3d\,^4P$	103.43	0.672(-5)	79.05	0.189(-7)	0.311(-7)
$2p^53p\,(^3P)3d\,^2P$	101.99	0.109(-8)	79.78	0.154(-6)	0.741(-8)
$2p^53p\,(^3S)3d\,^4D$	99.68	0.225(-13)	80.98	0.154(-10)	0.437(-8)
$2p^53s\,(^3P)3p\,^2S$	85.61	0.609(-2)	89.18	0.489(-8)	0.499(-7)
$2p^53s\,(^3P)3p\,^2P$	82.46	0.789(-4)	91.25	0.902(-7)	0.491(-7)
$2p^53s\,(^1P)3p\,^2S$	77.68	0.139(-4)	94.58	0.131(-6)	0.869(-8)
$2p^53s\,(^1P)3p\,^2P$	75.59	0.152(-5)	96.11	0.150(-6)	0.807(-10)
$2p^53s\,(^3P)3p\,^4P$	74.97	0.439(-5)	96.57	0.507(-8)	0.386(-10)
$2p^53s\,(^3P)3p\,^4D$	74.09	0.522(-7)	97.24	0.987(-8)	0.885(-12)

Even-parity states, $J=\frac{3}{2}$

Auger transitions to $2p^6\epsilon d$

$2p^53p\,(^1S)3d\,^2D$	113.23	0.319(-2)	74.40	0.353(-8)	0.147(-6)
$2p^53p\,(^3P)3d\,^2D$	109.83	0.190(-4)	75.95	0.331(-6)	0.106(-6)
$2p^53p\,(^3D)3d\,^2P$	108.95	0.135(-5)	76.36	0.423(-6)	0.520(-7)
$2p^53p\,(^1D)3d\,^2P$	107.08	0.901(-6)	77.25	0.211(-5)	0.860(-7)
$2p^53p\,(^3D)3d\,^2D$	106.94	0.102(-3)	77.32	0.133(-5)	0.951(-7)
$2p^53p\,(^1P)3d\,^2P$	105.81	0.481(-6)	77.87	0.101(-7)	0.753(-7)
$2p^53p\,(^3P)3d\,^4P$	105.68	0.121(-5)	77.93	0.669(-7)	0.557(-7)
$2p^53p\,(^1D)3d\,^2D$	105.52	0.183(-4)	78.01	0.572(-6)	0.755(-7)
$2p^53p\,(^3D)3d\,^4D$	105.03	0.114(-5)	78.25	0.730(-7)	0.831(-7)
$2p^53p\,(^3D)3d\,^4F$	104.68	0.268(-4)	78.42	0.305(-6)	0.618(-7)
$2p^53p\,(^1P)3d\,^2D$	104.51	0.350(-4)	78.51	0.261(-6)	0.537(-7)
$2p^53p\,(^3P)3d\,^4D$	103.96	0.272(-5)	78.78	0.116(-7)	0.692(-7)
$2p^53p\,(^3D)3d\,^4P$	103.53	0.158(-7)	79.00	0.357(-8)	0.515(-7)
$2p^53p\,(^3D)3d\,^4S$	103.09	0.258(-7)	79.22	0.891(-8)	0.288(-7)
$2p^53p\,(^3D)3d\,^2P$	102.66	0.466(-6)	79.44	0.769(-7)	0.108(-7)
$2p^53p\,(^3P)3d\,^4F$	102.36	0.104(-5)	79.59	0.549(-7)	0.769(-8)
$2p^53p\,(^3S)3d\,^2D$	101.38	0.316(-5)	80.09	0.622(-7)	0.113(-7)
$2p^53p\,(^3S)3d\,^4D$	99.77	0.752(-7)	80.94	0.161(-8)	0.488(-8)
$2p^53s\,(^3P)3p\,^2P$	82.29	0.198(-5)	91.36	0.801(-7)	0.475(-7)
$2p^53s\,(^3P)3p\,^2D$	81.52	0.292(-5)	91.88	0.718(-7)	0.459(-7)
$2p^53s\,(^1P)3p\,^2P$	75.84	0.587(-7)	95.92	0.146(-6)	0.866(-10)
$2p^53s\,(^1P)3p\,^2D$	75.31	0.196(-5)	96.31	0.968(-7)	0.191(-11)
$2p^53s\,(^3P)3p\,^4P$	74.79	0.677(-6)	96.70	0.464(-7)	0.671(-11)
$2p^53s\,(^3P)3p\,^4D$	73.87	0.165(-6)	97.41	0.109(-7)	0.786(-12)
$2p^53s\,(^3P)3p\,^4S$	72.19	0.354(-11)	98.71	0.829(-9)	0.985(-15)

Even-parity states, $J=\frac{5}{2}$

$2p^53p\,(^1S)3d\,^2D$	113.38	0.321(-2)	74.33	0.221(-7)	0.137(-6)
$2p^53p\,(^3P)3d\,^2F$	110.16	0.146(-4)	75.79	0.112(-6)	0.136(-6)
$2p^53p\,(^3P)3d\,^2D$	109.27	0.335(-5)	76.21	0.511(-6)	0.947(-7)
$2p^53p\,(^3D)3d\,^2D$	106.81	0.779(-4)	77.38	0.893(-6)	0.794(-7)
$2p^53p\,(^1D)3d\,^2D$	105.84	0.155(-4)	77.85	0.456(-6)	0.714(-7)
$2p^53p\,(^3P)3d\,^4P$	105.71	0.170(-5)	77.91	0.173(-7)	0.671(-7)

TABLE I. (Continued.)

Principal component	Auger transitions to $2p^6\epsilon d$ Energy	Rate	L-x-ray transition to $2p^63p$ Wavelength	Rate	Total M-x-ray rate
$2p^53p(^1D)3d\,^2F$	105.33	0.296(−7)	78.10	0.192(−8)	0.892(−7)
$2p^53p(^1P)3d\,^2D$	104.73	0.386(−4)	78.40	0.520(−6)	0.646(−7)
$2p^53p(^3D)3d\,^4F$	104.55	0.226(−4)	78.49	0.222(−6)	0.737(−7)
$2p^53p(^3D)3d\,^4D$	104.42	0.755(−5)	78.55	0.494(−7)	0.493(−7)
$2p^53p(^3P)3d\,^4D$	103.82	0.206(−5)	78.85	0.273(−8)	0.626(−7)
$2p^53p(^3D)3d\,^4P$	103.45	0.214(−6)	79.04	0.272(−8)	0.429(−7)
$2p^53p(^1P)3d\,^2F$	102.86	0.883(−6)	79.34	0.236(−7)	0.148(−7)
$2p^53p(^3P)3d\,^4F$	102.49	0.625(−7)	79.52	0.470(−8)	0.937(−8)
$2p^53p(^3D)3d\,^2F$	102.35	0.410(−6)	79.59	0.105(−7)	0.973(−8)
$2p^53p(^3S)3d\,^2D$	101.22	0.349(−5)	80.17	0.349(−7)	0.987(−8)
$2p^53p(^3D)3d\,^4G$	101.10	0.405(−7)	80.24	0.497(−9)	0.536(−8)
$2p^53p(^3S)3d\,^4D$	99.92	0.135(−6)	80.86	0.275(−8)	0.525(−8)
$2p^53s(^3P)3p\,^2D$	81.00	0.480(−5)	92.24	0.599(−7)	0.435(−7)
$2p^53s(^1P)3p\,^2D$	75.68	0.251(−5)	96.04	0.118(−6)	0.131(−10)
$2p^53s(^3P)3p\,^4P$	74.57	0.335(−6)	96.87	0.162(−7)	0.408(−12)
$2p^53s(^3P)3p\,^4D$	73.65	0.127(−6)	97.57	0.525(−8)	0.110(−11)

Even-parity states, $J=\frac{7}{2}$

Auger transitions to $2p^6\epsilon g$

Principal component	Energy	Rate			Total M-x-ray rate
$2p^53p(^3P)3d\,^2F$	110.05	0.451(−4)			0.130(−6)
$2p^53p(^3D)3d\,^2G$	108.91	0.207(−3)			0.125(−6)
$2p^53p(^1D)3d\,^2F$	105.63	0.550(−8)			0.932(−7)
$2p^53p(^3D)3d\,^4F$	104.45	0.224(−10)			0.710(−7)
$2p^53p(^3D)3d\,^4D$	104.30	0.158(−8)			0.546(−7)
$2p^53p(^3P)3d\,^4D$	103.69	0.826(−9)			0.576(−7)
$2p^53p(^1P)3d\,^2F$	102.84	0.286(−7)			0.187(−7)
$2p^53p(^3P)3d\,^4F$	102.52	0.370(−6)			0.758(−8)
$2p^53p(^1D)3d\,^2G$	101.77	0.188(−5)			0.124(−7)
$2p^53p(^3D)3d\,^2F$	101.62	0.906(−6)			0.108(−7)
$2p^53p(^3D)3d\,^4G$	100.87	0.524(−6)			0.151(−8)
$2p^53p(^3S)3d\,^4D$	100.13	0.263(−10)			0.598(−8)
$2p^53s(^3P)3p\,^4D$	73.48	0.157(−17)			0.000

Even-parity states, $J=\frac{9}{2}$

$2p^53p(^3D)3d\,^2G$	108.35	0.251(−3)			0.120(−6)
$2p^53p(^3D)3d\,^4F$	104.18	0.273(−7)			0.686(−7)
$2p^53p(^3P)3d\,^4F$	102.66	0.130(−5)			0.990(−8)
$2p^53p(^1D)3d\,^2G$	101.85	0.231(−5)			0.120(−7)
$2p^53p(^3D)3d\,^4G$	100.73	0.367(−6)			0.529(−8)

Even-parity states, $J=\frac{11}{2}$

| $2p^53p(^3D)3p\,^4G$ | | 0.000 | | | 0.470(−8) |

Odd-parity states, $J=\frac{1}{2}$

Principal component	Auger transitions to $2p^6\epsilon p$ Energy	Rate	L-x-ray transitions to $2p^63s$ Wavelength	Rate	$2p^63d$ Wavelength	Rate	Total M-x-ray rate
$2p^53d^2(^1S)\,^2P$	125.90	0.443(−5)	65.20	0.169(−8)	75.11	0.485(−6)	0.701(−7)
$2p^53d^2(^3P)\,^2P$	122.43	0.209(−4)	66.41	0.157(−8)	76.33	0.220(−5)	0.692(−7)
$2p^53d^2(^3P)\,^2S$	121.46	0.512(−6)	66.76	0.801(−10)	77.19	0.472(−7)	0.760(−7)
$2p^53d^2(^3P)\,^4D$	120.83	0.108(−5)	66.99	0.297(−9)	77.49	0.780(−7)	0.740(−7)
$2p^53d^2(^1D)\,^2P$	119.69	0.107(−5)	67.40	0.336(−8)	78.05	0.163(−8)	0.607(−7)
$2p^53d^2(^3P)\,^4P$	119.38	0.483(−9)	67.52	0.136(−9)	78.20	0.596(−8)	0.752(−7)
$2p^53d^2(^3F)\,^4D$	117.39	0.427(−8)	68.25	0.698(−13)	79.19	0.792(−9)	0.488(−7)
$2p^53p^2(^3P)\,^2P$	96.86	0.388(−2)	76.95	0.613(−6)	91.15	0.400(−7)	0.361(−7)
$2p^53s(^3P)3d\,^2P$	95.02	0.322(−2)	77.84	0.156(−5)	92.40	0.532(−7)	0.108(−6)
$2p^53s(^1P)3d\,^2P$	93.87	0.492(−4)	78.41	0.556(−6)	93.19	0.732(−7)	0.582(−7)
$2p^53p^2(^1S)3d\,^2P$	92.75	0.538(−3)	78.97	0.253(−7)	93.99	0.408(−7)	0.157(−7)

(Continued.) TABLE I.

Odd-parity states, $J = \frac{1}{2}$

| Principal component | Auger transitions to $2p^6\epsilon p$ | | L-x-ray transitions to | | | | Total M-x-ray rate |
| | Energy | Rate | $2p^6 3s$ | | $2p^6 3d$ | | |
			Wavelength	Rate	Wavelength	Rate	
$2p^5 3s(^3P)3d\ ^4D$	92.14	0.471(−5)	79.27	0.764(−7)	94.42	0.177(−7)	0.733(−7)
$2p^5 3s(^3P)3d\ ^4P$	90.38	0.500(−7)	80.18	0.156(−8)	95.71	0.172(−9)	0.705(−7)
$2p^5 3p^2(^3P)3d\ ^2S$	89.37	0.395(−5)	80.71	0.816(−10)	96.46	0.134(−10)	0.250(−7)
$2p^5 3p^2(^3P)3d\ ^4D$	88.26	0.240(−4)	81.29	0.738(−9)	97.30	0.113(−9)	0.252(−7)
$2p^5 3p^2(^1D)3d\ ^2P$	87.10	0.976(−4)	81.91	0.153(−7)	98.19	0.409(−8)	0.111(−7)
$2p^5 3p^2(^3P)3d\ ^4P$	86.90	0.781(−5)	82.02	0.312(−8)	98.35	0.976(−9)	0.210(−7)
$2p^5 3s^2(^1S)3d\ ^2P$	65.68	0.150(−4)	95.42	0.987(−7)	118.25	0.557(−10)	0.000

Odd-parity states, $J = \frac{3}{2}$.

Principal component	Energy	Rate	Wavelength	Rate	Wavelength	Rate	Total
$2p^5 3d^2(^1S)3d\ ^2P$	124.93	0.494(−5)	65.54	0.230(−8)	75.56	0.547(−6)	0.699(−7)
$2p^5 3d^2(^3P)3d\ ^2P$	122.75	0.202(−4)	66.30	0.477(−10)	76.57	0.215(−5)	0.676(−7)
$2p^5 3d^2(^3F)3d\ ^2D$	122.16	0.440(−6)	66.51	0.381(−12)	86.85	0.307(−5)	0.453(−7)
$2p^5 3d^2(^3P)3d\ ^4S$	121.40	0.111(−5)	66.78	0.602(−11)	77.21	0.916(−7)	0.775(−7)
$2p^5 3d^2(^3P)3d\ ^4D$	120.95	0.708(−6)	66.94	0.298(−11)	77.43	0.986(−7)	0.714(−7)
$2p^5 3d^2(^3P)3d\ ^2D$	120.41	0.468(−7)	67.14	0.859(−11)	77.70	0.481(−7)	0.730(−7)
$2p^5 3d^2(^1D)3d\ ^2P$	120.17	0.313(−6)	67.23	0.197(−9)	77.81	0.125(−6)	0.604(−7)
$2p^5 3d^2(^1D)3d\ ^2D$	119.38	0.463(−6)	67.52	0.412(−10)	78.20	0.542(−7)	0.572(−7)
$2p^5 3d^2(^3P)3d\ ^4P$	119.21	0.788(−10)	67.58	0.166(−10)	78.29	0.949(−8)	0.740(−7)
$2p^5 3d^2(^3F)3d\ ^4F$	118.54	0.142(−7)	67.82	0.678(−12)	78.62	0.828(−7)	0.456(−7)
$2p^5 3d^2(^3F)3d\ ^4D$	117.44	0.334(−8)	68.24	0.611(−13)	79.17	0.232(−8)	0.490(−7)
$2p^5 3p^2(^3P)3d\ ^2P$	97.38	0.256(−2)	76.70	0.184(−7)	90.80	0.427(−7)	0.598(−7)
$2p^5 3s(^3P)3d\ ^2D$	96.29	0.108(−2)	77.22	0.793(−9)	91.53	0.426(−7)	0.198(−7)
$2p^5 3s(^3P)3d\ ^2P$	94.91	0.364(−2)	77.90	0.470(−7)	92.48	0.444(−7)	0.306(−6)
$2p^5 3s(^1P)3d\ ^2P$	93.62	0.381(−3)	78.53	0.503(−6)	93.37	0.104(−6)	0.137(−6)
$2p^5 3s(^1P)3d\ ^2D$	92.98	0.169(−5)	78.85	0.443(−7)	93.82	0.113(−6)	0.477(−6)
$2p^5 3p^2(^1S)^2P$	92.43	0.116(−4)	79.13	0.143(−7)	94.22	0.189(−7)	0.237(−7)
$2p^5 3s(^3P)3d\ ^4D$	92.23	0.225(−6)	79.23	0.481(−7)	94.36	0.166(−7)	0.140(−6)
$2p^5 3s(^3P)3d\ ^4F$	91.48	0.513(−8)	79.61	0.378(−9)	94.90	0.884(−8)	0.164(−6)
$2p^5 3s(^3P)3d\ ^4P$	90.50	0.132(−6)	80.11	0.175(−8)	95.62	0.791(−9)	0.141(−6)
$2p^5 3p^2(^1D)^2D$	89.94	0.857(−5)	80.41	0.230(−12)	96.03	0.670(−8)	0.118(−7)
$2p^5 3p^2(^3P)^4S$	89.35	0.235(−4)	80.72	0.492(−9)	96.48	0.134(−9)	0.297(−7)
$2p^5 3p^2(^3P)^2D$	88.73	0.662(−5)	81.04	0.508(−9)	96.94	0.203(−8)	0.234(−7)
$2p^5 3p^2(^3P)^4D$	87.89	0.600(−5)	81.49	0.250(−9)	97.58	0.900(−9)	0.246(−7)
$2p^5 3p^2(^1D)^2P$	87.45	0.102(−3)	81.72	0.176(−7)	97.92	0.489(−8)	0.944(−8)
$2p^5 3p^2(^3P)^4P$	86.74	0.374(−6)	82.11	0.324(−9)	98.47	0.192(−9)	0.233(−7)
$2p^5 3s^2(^1S)^2P$	64.67	0.147(−4)	96.16	0.906(−7)	119.40	0.538(−10)	0.000

Odd-parity states, $J = \frac{5}{2}$

| Principal component | Auger transitions to $2p^6\epsilon f$ | | L-x-ray transitions to $2p^6 3d$ | | Total M-x-ray rate |
	Energy	Rate	Wavelength	Rate	
$2p^5 3d^2(^3F)^2D$	122.06	0.111(−4)	76.90	0.239(−5)	0.463(−7)
$2p^5 3d^2(^1G)^2F$	121.27	0.121(−2)	77.28	0.124(−5)	0.399(−7)
$2p^5 3d^2(^3P)^2D$	121.08	0.475(−3)	77.37	0.799(−6)	0.600(−7)
$2p^5 3d^2(^1D)^2F$	120.59	0.957(−3)	77.61	0.496(−6)	0.576(−7)
$2P^5 3d^2(^3P)^4D$	120.29	0.303(−4)	77.76	0.598(−8)	0.722(−7)
$2p^5 3d^2(^1D)^2D$	119.20	0.591(−4)	78.29	0.772(−7)	0.551(−7)
$2p^5 3d^2(^3F)^2F$	119.02	0.108(−3)	78.38	0.934(−8)	0.375(−7)
$2p^5 3d^2(^3P)^4F$	119.00	0.572(−5)	78.39	0.427(−8)	0.739(−7)
$2p^5 3d^2(^3F)^4F$	118.68	0.323(−6)	78.55	0.571(−7)	0.448(−7)
$2p^5 3d^2(^3F)^4G$	118.23	0.123(−6)	78.77	0.323(−7)	0.409(−7)
$2p^5 3d^2(^3F)^4D$	117.51	0.240(−6)	79.13	0.693(−8)	0.491(−7)
$2p^5 3s(^3P)3d\ ^2D$	96.45	0.545(−4)	91.42	0.488(−7)	0.334(−7)
$2p^5 3s(^3P)3d\ ^2F$	95.58	0.112(−3)	92.02	0.610(−7)	0.265(−7)
$2p^5 3s(^1P)3d\ ^2D$	93.16	0.426(−6)	93.70	0.111(−6)	0.759(−6)
$2p^5 3s(^1P)3d\ ^2F$	92.58	0.161(−5)	94.11	0.693(−7)	0.504(−6)

TABLE I. (*Continued.*)

| Principal component | Auger transitions to $2p^6\epsilon f$ | | L-x-ray transitions to $2p^63d$ | | Total M-x-ray rate |
	Energy	Rate	Wavelength	Rate	
			Odd-parity states, $J=\frac{5}{2}$		
$2p^53s(^3P)3d\,^4D$	92.06	0.949(−6)	94.48	0.549(−7)	0.435(−6)
$2p^53s(^3P)3d\,^4F$	91.26	0.143(−6)	95.06	0.987(−8)	0.251(−6)
$2p^53s(^3P)3d\,^4P$	90.72	0.201(−9)	95.47	0.243(−8)	0.217(−6)
$2p^53p^2(^1D)\,^2D$	89.88	0.254(−5)	96.08	0.628(−8)	0.149(−7)
$2p^53p^2(^3P)\,^2D$	89.13	0.374(−5)	96.64	0.752(−9)	0.201(−2)
$2p^53p^2(^1D)\,^2F$	88.73	0.789(−5)	96.94	0.479(−8)	0.115(−7)
$2p^53p^2(^3P)\,^4D$	87.69	0.722(−8)	97.74	0.217(−9)	0.253(−7)
$2p^53p^2(^3P)\,^4P$	86.56	0.129(−8)	98.61	0.110(−10)	0.236(−7)
			Odd-parity states, $J=\frac{7}{2}$		
$2p^53d^2(^1G)\,^2F$	121.94	0.139(−2)	76.96	0.116(−5)	0.239(−7)
$2p^53d^2(^1G)\,^2G$	121.08	0.760(−3)	77.37	0.696(−6)	0.246(−7)
$2p^53d^2(^3P)\,^4D$	120.20	0.237(−5)	77.80	0.184(−8)	0.693(−7)
$2p^53d^2(^1D)\,^2F$	119.84	0.597(−3)	77.98	0.190(−6)	0.610(−7)
$2p^53d^2(^3F)\,^2F$	119.22	0.840(−4)	78.28	0.294(−12)	0.370(−7)
$2p^53d^2(^3F)\,^4F$	118.99	0.131(−4)	78.39	0.239(−6)	0.409(−7)
$2p^53d^2(^3F)\,^2G$	118.41	0.236(−6)	78.68	0.780(−8)	0.434(−7)
$2p^53d^2(^3F)\,^4G$	118.06	0.245(−5)	78.86	0.802(−8)	0.333(−7)
$2p^53d^2(^3F)\,^4D$	117.65	0.264(−5)	79.07	0.681(−8)	0.497(−7)
$2p^53s(^3P)3d\,^2F$	95.09	0.165(−3)	92.35	0.703(−7)	0.304(−7)
$2p^53s(^1P)3d\,^2F$	92.86	0.401(−5)	93.91	0.905(−7)	0.837(−6)
$2p^53s(^3P)3d\,^4D$	91.88	0.654(−6)	94.61	0.248(−7)	0.420(−6)
$2p^53s(^3P)3d\,^4F$	91.05	0.115(−6)	95.21	0.491(−8)	0.307(−6)
$2p^53p^2(^1D)\,^2F$	88.26	0.142(−4)	97.30	0.316(−8)	0.832(−8)
$2p^53p^2(^3P)\,^4D$	87.49	0.109(−6)	97.89	0.144(−10)	0.259(−7)
			Odd-parity states, $J=\frac{9}{2}$		
		Auger transitions to $2p^6\epsilon h$			
$2p^53d^2(^1G)\,^2G$	121.41	0.952(−5)			0.199(−7)
$2p^53d^2(^1G)\,^2H$	120.18	0.520(−4)			0.193(−7)
$2p^53d^2(^3F)\,^2G$	119.26	0.712(−7)			0.431(−7)
$2p^53d^2(^3F)\,^4F$	118.30	0.413(−8)			0.438(−7)
$2p^53d^2(^3F)\,^4G$	117.92	0.185(−9)			0.436(−7)
$2p^53s(^3P)3d\,^4F$	90.86	0.000			0.347(−6)
			Odd-parity states, $J=\frac{11}{2}$		
$2p^53d^2(^1G)\,^2H$	119.63	0.616(−4)			0.191(−7)
$2p^53d^2(^3F)\,^4G$	117.81	0.399(−9)			0.450(−7)

Since total angular momentum and parity is conserved, two states with different angular momentum and parity cannot mix. Hence we grouped the 174 basis states ϕ_i according to their angular momentum and parity. This enabled us to break the 174×174 secular problem into a number of similar problems of smaller dimensions. The basis states ϕ_i and the mixing coefficients c_{ij} are not included in this paper but can be obtained from the authors on request.[18]

IV. RESULTS AND DISCUSSION

The calculated Auger-electron energies, x-ray wavelengths, and decay rates are listed in Table I. The initial states $\psi_i=\sum_j c_{ij}\phi_j$ are grouped according to angular momentum J and parity, and within each group they are arranged in order of decreasing energy. We indicate the dominant component of ψ_i in the first column; however, this identification should not be taken too seriously because in some cases two or more basis states contribute approximately equally. We do not list the energies and decay rates of M-x-ray transitions to individual final states, because of the huge number of possible final states. Instead, we only list the total rate of all M-x-ray transitions summed over final states.

A. Auger spectrum

The Auger spectrum produced in collisions of energetic phosphorus ions with carbon and argon has been mea-
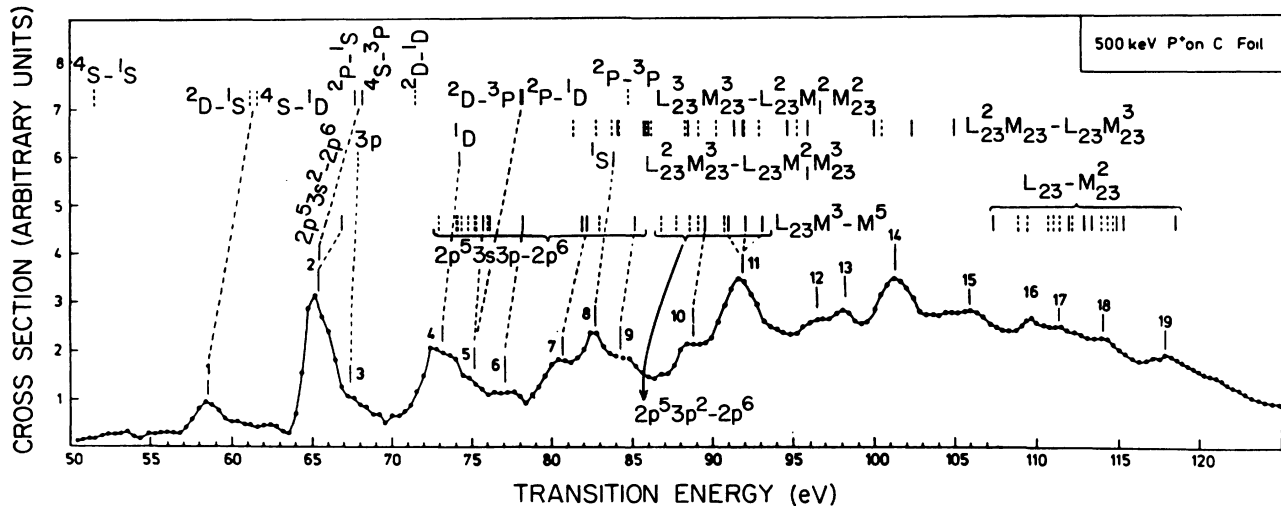
FIG. 1. Spectrum of phosphorus Auger electrons generated in the impact of 500-keV P^+ ions on carbon foil. From Ref. 1, by permission.

sured by Ridder and Schneider[1] and by Dahl et al.,[4] respectively. The spectrum can be analyzed on the basis of our calculated energies and transition rates.

The Auger spectrum from 500-keV P^+ impact on C foil is reproduced in Fig. 1. Ridder and Schneider[1] have identified lines 1 through 11 of this spectrum on the basis of their single-particle calculations of term energies, without configuration interaction. We agree with the assignments of Ref. 1, except for the transitions $2p^53s3p(^3P)(^{2S+1}L) \to 2p^6(^1S)$ (line 4) and $2p^53p^2(^1D),(^3P), \, ^2P \to 2p^6(^1S)$ (line 11). In addition. we can identify lines 12 through 19 from the present calculations and can make more specific assignments. Configuration interaction and intermediate coupling furthermore introduce many new terms that are forbidden in LS coupling; these additional transitions are also assigned to the observed lines. In Table II we list energies and decay rates calculated in intermediate coupling with configuration interaction and, for comparison, in LS coupling, for some of the important transitions. Both our assignments of lines to these transitions and those of Ridder and Schneider[1] are indicated. Configuration interaction and intermediate coupling are found to produce better agreement with the observed spectrum.

A few specific comments are appropriate here. In Fig. 1, line 2 is seen to be well separated from neighboring Auger peaks; this line can clearly be assigned to the transition $2p^53s^2 \, ^2P \to 2p^6(^1S)$. Furthermore, as pointed out by Ridder and Schneider,[1] transitions of the type $2p^33s^2 \, ^2P \to 2p^4(^1S)$ and $2p^33s^2 \, ^4S \to 2p^4(^3P)$ may also contribute to line 2. Line 4 is produced by the transitions $2p^53s(^3P)3p \, ^4D_{1/2,3/2,5/2}, \, ^4S_{3/2} \to 2p^6(^1S)$, which are not allowed in LS coupling. Line 5 can be assigned to transitions $2p^53s(^1P)3p \, ^2D_{3/2,5/2} \to 2p^6(^1S)$. These two lines are quite close together, and the transition $2p^53s(^3P)3p \, ^4P_{1/2,3/2,5/2} \to 2p^6(^1S)$ with intermediate energy may contribute to either of these lines.

Each of the lines 6–9, 12, 13, 15, and 17–19 is produced by several transitions, as described in Tables I and II. Line 8 is due to transitions $2p^53s(^3P)3p \, ^2P_{1/2,3/2} \to 2p^6(^1S)$, which are forbidden in LS coupling. The transition $2p^43s^2 \, ^1S \to 2p^5(^2P)$ may also contribute to this line.[1] In the case of line 10 we can expect some contribution from the transitions $2p^53p^2(^3P)^4D_{1/2} \to 2p^6(^1S)$.

Lines 11 and 14 are broad, and looking at Table I we can find a multitude of transitions that contribute to these peaks. We are unable to identify lines 1 and 3, which cannot originate from the configurations considered here. A tentative assignment for line 1 has been offered in Ref. 1.

B. X-ray emission spectrum

The L-x-ray spectrum of multiply stripped phosphorus from 100-keV P^+ + Ar collisions has been measured by Peterson et al.[2] (Fig. 2). The structure of the spectrum is complex, with lines clustering in groups. In Ref. 2, specific assignments for some peaks have been made and tentative identifications are offered for others, while certain lines and groups of lines remain unidentified. We can analyze the x-ray spectrum on the basis of the present theoretical x-ray wavelengths and transition rates. The calculated wavelengths are seen to fall into certain groups that can be identified with observed groups of lines of the phosphorus spectrum.

The lines clustered between 90 and 98 Å are mainly due to the transitions $2p^53s3p \to 2p^63p$, $2p^53s3d \to 2p^63d$, and $2p^53s^2 \to 2p^63s$. The two intense lines near 91 Å cannot arise from these transitions alone, although they will contain contributions from them. The prominent lines around 96 Å are due to $2p^53s(^1P)3p \, ^2P_{1/2,3/2} \to 2p^63p \, ^2P$ and $2p^53s(^1P)3p \, ^2D_{3/2,5/2} \to 2p^63p$ transitions. These transitions are characterized by large L-shell fluorescence yields. The line near 94.6 Å can arise from the

TABLE II. Assignments of prominent transitions in the P^{4+} Auger spectrum. Line numbers refer to peaks in the spectrum shown in Fig. 1. Energies are in eV and rates in atomic units. Numbers in parentheses indicate powers of 10.

Initial state	LS Energy	Coupling Rate	Intermediate coupling with config. interaction		Proposed assignment (line number)	
			Energy	Rate	Present	Ref. 1.
$2p^5 3s^2(^1S)^2P_{1/2}$	66.38	0.870(-4)	65.88	0.150(-4)	2	2
$^2P_{3/2}$			64.67	0.147(-4)		
$2p^5 3s(^3P)3p\,^4D_{1/2}$			74.09	0.522(-7)		
$^4D_{3/2}$			73.87	0.165(-6)	4	
$^4D_{5/2}$			73.65	0.127(-6)		
$2p^5 3s(^1P)3p\,^2D_{3/2}$	75.47	0.154(-6)	75.31	0.196(-5)	5	5
$^2D_{5/2}$			75.68	0.251(-5)		
$^2S_{1/2}$	77.73	0.384(-4)	77.68	0.139(-4)	6	6
$2p^5 3s(^3P)3p\,^2D_{3/2}$	81.49	0.102(-5)	81.52	0.292(-5)	7	7
$^2D_{5/2}$			81.00	0.480(-5)		
$^2S_{1/2}$	85.78	0.624(-2)	85.61	0.609(-2)	9	9
$2p^5 3p^2(^1D)^2P_{1/2}$	88.11	0.264(-4)	87.10	0.976(-4)		11
$^2P_{3/2}$			87.45	0.102(-3)	10	
$^2F_{5/2}$	89.89	0.106(-3)	88.73	0.789(-5)		10
$^2F_{7/2}$			88.26	0.142(-4)		
$2p^5 3p^2(^1S)^2P_{1/2}$	93.30	0.179(-6)	92.75	0.538(-3)		11
$^2P_{3/2}$			92.43	0.116(-4)		
$2p^5 3s(^1P)3d\,^2F_{5/2}$	92.46	0.226(-4)	92.58	0.161(-5)	11	
$^2F_{7/2}$			92.86	0.401(-5)		
$2p^5 3s(^3P)3d\,^2D_{3/2}$			96.29	0.108(-2)		
$^2D_{5/2}$			96.45	0.545(-4)	12	
$2p^5 3p^2(^3P)^2P_{1/2}$	96.34	0.724(-2)	96.86	0.388(-2)	13	11
$^2P_{3/2}$			97.38	0.256(-2)		
$2p^5 3p(^3S)3d\,^2D_{3/2}$	101.46	0.399(-5)	101.38	0.316(-5)	14	
$^2D_{5/2}$			101.22	0.349(-5)		
$2p^5 3p(^1D)3d\,^2S_{1/2}$	105.77	0.143(-3)	106.21	0.223(-3)		
$^2D_{3/2}$	105.46	0.275(-4)	105.52	0.183(-4)		
$^2D_{5/2}$			105.84	0.155(-4)	15	
$2p^5 3p(^3D)3d\,^2D_{3/2}$	106.83	0.830(-4)	106.94	0.102(-3)		
$^2D_{5/2}$			106.81	0.779(-4)		
$2p^5 3p(^3P)3d\,^2D_{3/2}$	109.40	0.249(-5)	109.83	0.190(-4)	16	
$^2D_{5/2}$			109.27	0.335(-5)		
$2p^5 3p(^3P)3d\,^2F_{5/2}$			110.16	0.146(-4)		
$^2F_{7/2}$			110.05	0.451(-4)	17	
$2p^5 3p(^1S)3d\,^2D_{3/2}$	113.26	0.323(-2)	113.23	0.319(-2)		
$^2D_{5/2}$			113.38	0.321(-2)	18	
$2p^5 3d^2(^3F)^2F_{5/2}$	118.96	0.646(-4)	119.02	0.108(-3)		
$^2F_{7/2}$			119.22	0.840(-4)	19	

$2p^5 3s(^1P)3p\,^2S \rightarrow 2p^6 3p\,^2P$ transition.

The group of lines between 73 and 80 Å can arise from the transitions $2p^5 3s\,3d \rightarrow 2p^6 3s$, $2p^5 3p\,3d \rightarrow 2p^6 3p$, $2p^5 3p^2 \rightarrow 2p^6 3s$, and $2p^5 3d^2 \rightarrow 2p^6 3d$. The line at ~ 79.5 Å is due to $2p^5 3p(^3P)3d\,^2P_{1/2,3/2} \rightarrow 2p^6 3p\,^2P$. The 77.4- Å line is produced by $2p^5 3p(^1D)3d\,^2P_{1/2,3/2} \rightarrow 2p^6 3p\,^2P$ transitions and the lines near 76 Å are due to $2p^5 3p(^3D)3d\,^2S \rightarrow 2p^6 3p\,^2P$ and $2p^5 3p(^3P)3d\,^2D_{3/2,5/2} \rightarrow 2p^6 3p\,^2P$. No lines between 82 and 89 Å and between 68.5 and 74 Å can arise from the configurations considered in this paper.

In the x-ray spectrum we can identify comparatively fewer lines than in the Auger spectrum, because some of the prominent x-ray lines arise from configurations of the type $2p^5 3l$ or $2p^4 3l$, not included in the present calculations. The excitation cross section for these configurations is smaller than for $2p^5 3s^n 3p^m$ configurations by about two orders of magnitude,[2] but they can decay only by L-x-ray emission. Peterson et al.[2] based their assignments mainly on this type of configurations, and their assignments thus complement ours.

The dipole selection rule does not allow the even-parity states with $J > \frac{5}{2}$ to decay by L-x-ray emission. The same holds for odd-parity states with $J > \frac{7}{2}$. The quartet states are fairly long lived. Intermediate coupling allows them to decay by Auger and L-x-ray emission; the total L- and M-x-ray decay rates of these states are comparable. The particular state $2p^5 3p(^3D)3d\,^4G_{11/2}$ can decay only by M-
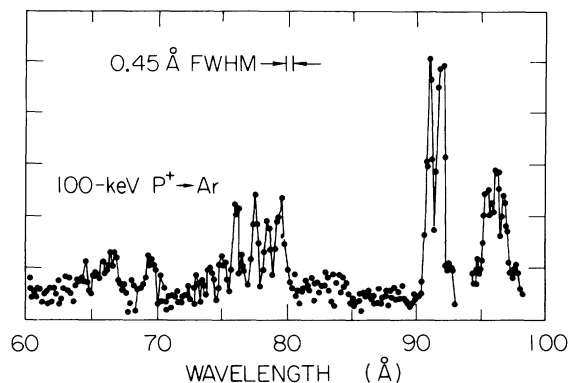
FIG. 2. Phosphorus L-x-ray spectrum from $P^+ + Ar$ collisions. Intensities are relative and have not been corrected for window absorption. Adapted from Ref. 2, by permission.

$2p^53p3d \rightarrow 2p^53s\,3d$, and $2p^53p3d \rightarrow 2p^53p^2$. The populations of certain states can thus be boosted.

V. CONCLUSIONS

The Auger and L-x-ray spectra from multiply stripped P^{4+} ions following ion-atom collisions have been analyzed on the basis of calculated energies and decay rates. Transitions from $2p^53s^2$, $2p^53s3p$, and $2p^53p^2$ (outside the Be core) are found to contribute mainly to the low-energy part of the Auger spectrum, while the configurations $2p^53p\,3d$ and $2p^53s\,3d$ contribute to the higher-energy segment. Transitions from the latter two configurations also produce some prominent x-ray lines. The effect of configuration interaction on energies and decay rates is large: Level energies can be shifted by as much as 1.5 eV, and the decay rates can be changed by an order of magnitude.

ACKNOWLEDGMENTS

x-ray emission and is long lived. Cascade feeding to some of the initial configurations is possible through certain M-x-ray transitions, as for example $2p^53d^2 \rightarrow 2p^53p\,3d$, $2p^53p^2 \rightarrow 2p^53s3p$, $2p^53s3p \rightarrow 2p^53s^2$, $2p^53s\,3d \rightarrow 2p^53s\,3p$,

[1]D. Ridder and D. Schneider, Phys. Rev. A 25, 921 (1982).
[2]R. S. Peterson, W. W. Smith, H. C. Hayden, and M. Furst, IEEE Trans. Nucl. Sci. NS-28, 1114 (1981).
[3]R. S. Peterson, W. W. Smith, H. C. Hayden, and M. Furst, Bull. Am. Phys. Soc. 25, 1125 (1980).
[4]P. Dahl, M. Rodbro, G. Herman, B. Fastrup, and M. E. Rudd, J. Phys. B 9, 1581 (1976).
[5]D. Chatterji, The Theory of Auger Transitions (Academic, New York, 1976).
[6]M. H. Chen, B. Crasemann, and H. Mark, Phys. Rev. A 21, 442 (1980).
[7]M. H. Chen, B. Crasemann, and H. Mark, Phys. Rev. A 24, 1852 (1981).
[8]M. H. Chen, B. Crasemann, K. R. Karim, and H. Mark, Phys. Rev. A 24, 1845 (1981).

[9]M. H. Chen and B. Crasemann, Phys. Rev. A 12, 959 (1975).
[10]C. P. Bhalla, Phys. Rev. A 12, 122 (1975).
[11]G. Racah, Phys. Rev. 63, 367 (1943).
[12]U. Fano, Phys. Rev. 140, A67 (1965).
[13]N. Rosenzweig, Phys. Rev. 88, 580 (1952).
[14]I. I. Sobelman, Introduction to the Theory of Atomic Spectra (Pergamon, New York, 1972).
[15]A. Hibbert, Comput. Phys. Commun. 2, 180 (1971).
[16]F. Herman and S. Skillman, Atomic Structure Calculations (Prentice-Hall, Englewood Cliffs, N. J., 1963).
[17]B. G. Wybourne, Spectroscopic Properties of Rare Earths (Wiley, New York, 1965).
[18]K. R. Karim, Ph.D. thesis, University of Oregon, 1983 (unpublished).